

NASA Technical Memorandum 4174

# **Analysis and Testing of Axial Compression in Imperfect Slender Truss Struts**

**Mark S. Lake and Nicholas Georgiadis**

**FEBRUARY 1990**

**NASA**

## Summary

This study addresses the axial compression of imperfect slender struts for large space structures. The load-shortening behavior of struts with initially imperfect shapes and eccentric compressive end loading is analyzed using linear beam-column theory and results are compared with geometrically nonlinear solutions to determine the applicability of linear analysis. A set of aluminum-clad graphite/epoxy struts sized for application to the Space Station Freedom truss are measured to determine their initial imperfection magnitude, load eccentricity, and cross-sectional area and moment of inertia. Load-shortening curves are determined from axial compression tests of these specimens and are correlated with theoretical curves generated using linear analysis.

## Introduction

The Space Station Freedom represents the first of a new generation of spacecraft whose components will be assembled on-orbit and integrated within a large lightweight truss structure (see fig. 1). Recent studies (refs. 1 and 2) have resulted in the selection of a 5-m erectable design as the baseline configuration for this structure. Advanced development programs (refs. 3, 4, and 5) underway for a number of years have resulted in the fabrication of high-stiffness aluminum-clad graphite/epoxy truss struts (see fig. 2) and the development of quick-attachment erectable joints (see fig. 3).

The depth of the space station truss structure (5 m) was selected primarily because of stiffness instead of strength considerations. Low packaged-volume constraints have dictated the use of very long, slender struts. However, the structure is also required to withstand significant loads due to thermal gradients, spacecraft operations, and attitude control maneuvers. Consequently, elastic stability of these slender struts is a design concern.

Previous studies (refs. 6 and 7) addressed the elastic stability of long slender struts for general large space structure applications. This paper summarizes the results of a study that extends this previous work and specifically addresses the effect of geometric irregularities encountered during development of the aluminum-clad graphite/epoxy struts. Such irregularities are common to the fabrication of long slender struts by most manufacturing processes. The load-shortening behavior of initially curved struts with eccentric compressive end loading is studied herein analytically using both linear and nonlinear beam theory. Results from these analyses are compared to determine the applicability of linear analysis. Several struts produced during development of the strut fabrication process are measured to determine cross-sectional variations and imperfections in straightness. Finally, results from compression tests of these specimens are correlated with results generated using linear analysis.

## Symbols

$A$	cross-sectional area
DCDT	direct current differential transformer
$E$	Young's modulus
$e$	applied load eccentricity
$I$	cross-sectional moment of inertia
$I_p$	moment of inertia of cross section with no concentricity error
$l$	strut length
$l^*$	distance between reference points for axial shortening measurements
$P$	axial compressive load on strut

$P_e$	Euler buckling load of strut
$P_{ep}$	Euler buckling load of perfect strut
$q$	ratio of axial compression load to Euler buckling load
$q_l$	limit load for applicability of linear analysis
$q_{\max}$	maximum load applied in compression test
$r_i$	inner radius of strut cross section
$r_o$	outer radius of strut cross section
$t$	average thickness of strut cross section
$t_{\min}$	minimum thickness of strut cross section
$t_{\max}$	maximum thickness of strut cross section
$\Delta t$	difference in minimum and maximum thicknesses of strut cross section
$u$	longitudinal displacement of strut
$w$	lateral displacement of strut
$w_h$	homogeneous portion of lateral displacement solution
$w_o$	initial imperfection of strut
$x, y, z$	Cartesian coordinates
$x_0$	longitudinal position of first reference point for axial shortening measurements
$x_1$	longitudinal position of second reference point for axial shortening measurements
$y_i$	distance from centroid to center of inside surface of eccentric cross section (see fig. 9)
$y_o$	distance from centroid to center of outside surface of eccentric cross section (see fig. 9)
$\delta$	total axial shortening of strut
$\varepsilon$	magnitude of strut initial imperfection at strut midlength
$\Delta\varepsilon_{\text{rms}}$	percent-rms difference between measured imperfections and best-fit parabolic curve

### Analysis of Axial Shortening of Eccentrically Loaded, Imperfect Struts

The deformed shape  $w(x)$  of a strut with an initial imperfection  $w_o(x)$  and acted on by a Compressive axial load  $P$  applied at a distance  $e$  from the neutral axis is shown in figure 4. The linear differential equation and the appropriate boundary conditions to determine  $w(x)$  are given in equation (1) and are derived in ref. 8.

$$EI \frac{d^2 w}{dx^2} + Pw = -P(w_o + e) \quad (1)$$

where

$$w(0) = w(L) = 0$$

The solution to the homogeneous portion of equation (1) is

$$w_h = B_1 \cos\left(\pi\sqrt{q}\frac{x}{l}\right) + B_2 \sin\left(\pi\sqrt{q}\frac{x}{l}\right) \quad (2)$$

where  $B_1$  and  $B_2$  are determined from the boundary conditions and  $q$ , the compressive axial load normalized by the Euler buckling load for the simply supported strut, is defined as

$$q = \frac{P}{P_e} = \frac{Pl^2}{\pi^2 EI} \quad (3)$$

The initial imperfection  $w_o(x)$  is assumed to be parabolic with a maximum magnitude of  $\varepsilon$ , and is given by

$$w_o = 4\varepsilon \left[ \frac{x}{l} - \left( \frac{x}{l} \right)^2 \right] \quad (4)$$

Substituting equation (4) into equation (1), determining the particular solution, and applying the boundary conditions, results in the following expression for lateral displacement of a compressively loaded strut with a parabolic initial imperfection:

$$w(x) = \frac{8\varepsilon}{\pi^2 q} \left( \frac{\pi^2 q x^2}{2l^2} - \frac{\pi^2 q x}{2l} - 1 \right) + \left( \frac{8\varepsilon}{\pi^2 q} + e \right) \left[ \tan \left( \frac{\pi \sqrt{q}}{2} \right) \sin \left( \frac{\pi \sqrt{q} x}{2} \right) + \cos \left( \frac{\pi \sqrt{q} x}{2} \right) \right] - e \quad (5)$$

For small lateral displacements, total axial shortening can be calculated by superimposing the contribution due to uniform axial compression on that due to lateral displacement. The axial shortening between any two arbitrary points  $x_0$  and  $x_1$  is found by integrating the axial strain between these limits. In order to represent both the effect of uniform axial compression and the effect of lateral displacement, it is necessary to include both the linear term and the first nonlinear term of axial strain. The equation for axial shortening is thus

$$\delta = \frac{1}{2} \int_{x_0}^{x_1} \left[ \frac{du}{dx} + \frac{1}{2} \left( \frac{dw}{dx} \right)^2 \right] dx = \int_{x_0}^{x_1} \frac{du}{dx} dx + \frac{1}{2} \int_{x_0}^{x_1} \left( \frac{dw}{dx} \right)^2 dx \quad (6)$$

To determine the axial shortening of a strut with an initial lateral imperfection  $w_o(x)$  equation (6) must be modified. In this case the total lateral displacement after application of load is  $w(x) + w_o(x)$  (see fig. 4). Therefore, the axial shortening due to the elastic deflection  $w(x)$  is

$$\delta = \int_{x_0}^{x_1} \frac{du}{dx} dx + \frac{1}{2} \int_{x_0}^{x_1} \left[ \frac{d(w_o + w)}{dx} \right]^2 dx - \frac{1}{2} \int_{x_0}^{x_1} \left( \frac{dw_o}{dx} \right)^2 dx \quad (7)$$

The linear strain in the first term of equation (7) is the uniform axial compressive stress divided by the Young's modulus of the strut. Making this substitution and evaluating the first integral gives

$$\delta = \frac{Pl^*}{EA} + \frac{1}{2} \int_{x_0}^{x_1} \left[ \frac{d(w_o + w)}{dx} \right]^2 dx - \frac{1}{2} \int_{x_0}^{x_1} \left( \frac{dw_o}{dx} \right)^2 dx \quad (8)$$

where  $l^* = x_1 - x_0$

The remaining two terms in equation (8) can now be evaluated by substitution of the parabolic initial imperfection  $w_o$  given in equation (4) and the corresponding lateral displacement  $w$  given in equation (5). The following integral expression is obtained:

$$\delta = \left( \frac{32\varepsilon^2}{\pi^2 q l^2} + \frac{8\varepsilon e}{l^2} + \frac{\pi^2 q e^2}{2l^2} \right) \int_{x_0}^{x_1} \left[ \tan^2 \left( \frac{\pi \sqrt{q}}{2} \right) \cos^2 \left( \frac{\pi \sqrt{q} x}{2} \right) - 2 \tan \left( \frac{\pi \sqrt{q}}{2} \right) \cos \left( \frac{\pi \sqrt{q} x}{2} \right) \sin \left( \frac{\pi \sqrt{q} x}{2} \right) + \sin^2 \left( \frac{\pi \sqrt{q} x}{2} \right) - \frac{8\varepsilon^2}{4} (l^2 - 4xl + 4x^2) \right] dx + \frac{Pl^*}{EA} \quad (9)$$

The total axial shortening of the strut can be determined by setting  $x_0 = 0$  and  $x_0 = l$  in equation (9). Integration and simplification of this equation lead to the following expression:

$$\delta = \varepsilon^2 \left\{ \frac{32[\pi\sqrt{q} - \sin(\pi\sqrt{q})]}{l(\pi\sqrt{q})^3[1 + \cos(\pi\sqrt{q})]} - \frac{8}{3l} \right\} + \varepsilon e \left\{ \frac{8[\pi\sqrt{q} - \sin(\pi\sqrt{q})]}{l\pi\sqrt{q}[1 + \cos(\pi\sqrt{q})]} \right\} + e^2 \left\{ \frac{\pi\sqrt{q}[\pi\sqrt{q} - \sin(\pi\sqrt{q})]}{2l[1 + \cos(\pi\sqrt{q})]} \right\} + \frac{Pl}{EA} \quad (10)$$

Equation (10) is the sum of four terms that make specific contributions to the axial shortening of the strut. The first term is due solely to the initial imperfection. The second term accounts for the interaction between initial imperfection and load eccentricity. The third term is due solely to the load eccentricity. Finally, the fourth term is the contribution due to uniform axial compression.

It is common in linear imperfect strut analysis to assume a half-sine rather than a parabolic initial imperfection shape because the homogeneous solution to the differential equation is already of this form (see eq. (2)). Although the study is based on a parabolic initial imperfection, a derivation of the equation for axial shortening of a strut with a half-sine initial imperfection is presented in appendix A.

Of concern in the analysis of axial shortening of eccentrically loaded columns with initial imperfections is the occurrence of large deflections and the importance of geometric nonlinearities. The nonlinear solution for end shortening of an eccentrically loaded column with a circular initial imperfection is presented in reference 9. This solution is inherently transcendental and requires the use of numerical iteration routines. Consequently, it is desirable to use the linear solution presented in equation (10) for problems involving sufficiently small deflections. A comparison of results from equation (10) with results from the nonlinear solution are presented in appendix B. From this comparison, loads are defined where the linear solution departs from the nonlinear solution by a specified percentage for ranges of the initial imperfection and load eccentricity magnitudes.

## Testing of Imperfect Slender Truss Struts

Eleven struts, sized for application to the Space Station Freedom truss, were tested to determine their load-shortening behavior. Nine of the specimens were 5 m long and two of the specimens were 7.1 m long. Before loading, each specimen was measured to determine its initial imperfection and cross-sectional uniformity. Descriptions of the test setup and imperfection measurements of the specimens are presented in this section. Finally, experimental load-shortening data are presented for each specimen and compared with analytical predictions based on the linear analysis developed in the preceding section.

### Description of Test Setup

Before testing, each specimen was mated to quick-attachment erectable joint hardware of the type shown in figure 3, and the assembly was accurately set to length. The specimen was mounted vertically between a hydraulic jack for load introduction and a load cell for load measurement. This test setup is diagramed in figure 5 and shown in figure 6.

Centerline shortening of each specimen was determined from direct current differential transformer (DCDT) measurements made at two stations along the length of the specimen ( $x_0$  and  $x_1$  inches from the bottom of the specimen). These locations spanned the portion of the strut with a uniform cross-sectional area, thus displacement measurements between them excluded any deformation in the erectable end-joints. Displacement at the center of the specimen cross section was calculated by averaging the readings of three DCDT's located at the

apexes of an equilateral triangle centered on the cross section. This process eliminates the effects of local bending rotations in the specimen regardless of the direction of rotation. The approximate location of the measurement stations and a section view of the upper station showing the DCDT placement are shown in figure 5. The axial shortening of the specimen between these two stations is determined by subtracting the centerline displacement at the upper station (DCDT s 1, 2, and 3) from the centerline displacement at the lower station (DCDT s 4, 5, and 6).

Details of the fixture used to provide a pinned-end restraint to the specimen are shown in figure 7. The left-hand photograph shows the lower end of the specimen, the lower DCDT station, and the hydraulic jack. The right-hand photograph shows a close-up view of the specimen end fixture. A special joint adaptor was attached to the node fitting portion of the erectable joint to cause end rotation of the specimen to occur at the theoretical node center (see fig. 3). Because of the arbitrary orientation of initial imperfections and eccentricities, it was impossible to identify, a priori, the preferred direction of buckling of the specimens. Therefore, it was necessary to provide an omnidirectional pinned-end restraint by incorporating a hemispherical end on the joint adaptor and a mating hemispherical socket in the hydraulic jack adaptor. A thin sheet of greased Teflon was inserted between these adaptors to ensure a low-friction interface. Identical fixtures were used on both the top and the bottom of the specimen.

The initial imperfections of the specimens were determined from lateral DCDT measurements made along the strut length. Measurements were made at evenly spaced stations as the specimen was rotated 360° around its longitudinal axis. The lower lateral DCDT (DCDT 9) and a series of indicator marks to locate the orientation angle around the circumference of the specimen are shown in figure 8. An explanation of the procedure used to determine initial imperfection magnitudes from these readings is presented in the following section.

### Description of Specimens

Each specimen was measured to determine an initial imperfection magnitude and variations in its cross-sectional dimensions. Results of these measurements are presented below.

***Specimen initial imperfection magnitudes.*** The initial imperfection was measured at three points along the length of the specimen: 0.25*l*, 0.50*l*, and 0.75*l*. To determine the imperfection values at each point, DCDT readings were taken at 20° increments as the strut was rotated about its longitudinal axis. The minimum reading was then subtracted from the maximum reading with the result divided by two to give the imperfection value at this point. These values for the imperfection at the three span locations were used to obtain a least-squares regression fit of equation (4). The resulting expression for the best-fit  $\epsilon$  is given in equation (11):

$$\epsilon = \frac{2}{17} (3w_{1/4} + 4w_{1/2} + 3w_{3/4}) \quad (11)$$

where  $w_{1/4}$ ,  $w_{1/2}$ ,  $w_{3/4}$  are the measured values of imperfection at 0.25*l*, 0.50*l*, and 0.75*l*, respectively.

To determine the quality of the parabolic curve fit of the imperfection data, the percent-rms difference ( $\Delta\epsilon_{\text{rms}}$ ) between the data and the best-fit parabolic curve is also calculated. These results are presented in table I along with the specimen lengths and the location of the upper and lower stations for measuring axial displacement (see fig. 5). The parabolic curve fit approximations to the actual imperfection shape of the specimens were found to exhibit rms errors between 1.8 and 26 percent.

Table I. Specimen Lengths and Initial Imperfections

Specimen	$l$ , in.	$x_0$ , in.	$x_1$ , in.	$l^*$ , in.	$\epsilon$ , in.	$\Delta\epsilon_{\text{rms}}$ , %
1	196.8	8.1	188.7	180.6	0.071	26.0
2	196.8	8.1	188.7	180.6	.307	8.8
3	196.8	8.1	188.7	180.6	.187	16.6
4	196.8	8.1	188.7	180.6	.232	8.0
5	196.8	8.1	188.7	180.6	.215	10.8
6	196.8	8.1	188.7	180.6	.145	10.7
7	196.8	8.1	188.7	180.6	.265	10.0
8	196.8	8.1	188.7	180.6	.214	1.8
<sup>a</sup> 9	196.8	8.5	186.9	178.4	.075	15.0
10	278.4	8.1	270.3	262.2	.681	3.2
11	278.4	8.1	270.3	262.2	.382	9.6

<sup>a</sup>The values of  $x_0$  and  $x_1$  for specimen 9 are different from those for the other 5-m struts because of a manufacturing error that necessitated the addition of a tubular aluminum extension to one end of the specimen.

**Specimen cross-sectional variations.** Ideally, the inner and outer layers of aluminum in the strut cross section (see fig. 2) should be concentric and of constant thickness as should the layer of graphite/epoxy. The nominal design values for the thicknesses of each aluminum layer, the thickness of the graphite/epoxy layer, and the outer radius are 0.006, 0.060, and 1.066 in., respectively.

The specimen cross sections showed a lack of concentricity between the inner and outer layers of aluminum and thus, significant variations from the nominal dimensions. This lack of concentricity results in a shift of the centroid of the cross section, and thus, a reduction in the moment of inertia and the introduction of a load eccentricity. In general, it was observed that the cross-sectional imperfections were aligned with the initial imperfection bow in the strut such that all effects (load eccentricity, reduced cross-sectional moment of inertia, and initial strut bow) were additive in degrading the load-shortening performance of the strut.

Measurements of outside diameter and wall thickness were made at various orientations around both ends of each specimen and these values were used to derive average cross-sectional properties. For the purpose of these calculations, the three-layer, two-material, annular cross section was assumed to be a single-layer, one-material annular cross section with an effective Young's modulus to be determined from experiment.

A strut cross section in which the inner and outer circular surfaces are not concentric is shown in figure 9. The axes shown are centroidal and the distances to the centers of the inner and outer circular surfaces from the origin are defined as  $y_i$  and  $y_o$ , respectively. The radii of these inner and outer surfaces are  $r_i$  and  $r_o$ , respectively, and the minimum and maximum thicknesses are  $t_{\min}$  and  $t_{\max}$ , respectively. The difference in the minimum and maximum thicknesses is given by

$$\Delta t = t_{\max} - t_{\min} = 2(y_i - y_o) \quad (12)$$

The average thickness,  $t$ , is defined to be

$$t = \frac{1}{2}(t_{\max} + t_{\min}) \quad (13)$$

From the definition of the centroid of a planar region, it follows that

$$\int_{Area} y dA = 0 \Rightarrow y_o r_o^2 = y_i r_i^2 \quad (14)$$

During manufacture, the inside of the ends of each tube was machined on a lathe to accept a tapered, bonded adaptor fitting for the erectable joint hardware. The center of machining was the center of the outside surface of the strut cross section. Therefore, after assembly, the center of the hemispherical end of the joint adaptor fitting (see fig. 7) was coincident with the center of the outside surface. Accordingly, the center of the outside surface was assumed to be the point of application of the load, and therefore the load eccentricity  $e$  is given by the following equation (see fig. 9):

$$e = y_o \quad (15)$$

Substituting equations (12) through (14) into equation (15) and simplifying gives the following expression for load eccentricity in terms of the outer radius, the average thickness, and the difference between the maximum and minimum thicknesses:

$$e = \frac{\Delta t (r_o^2 - 2r_o t + t^2)}{2(2r_o t - t^2)} \quad (16)$$

To quantify the concentricity effect, the eccentricity given by equation (16) can be expressed as a function of the concentricity error ( $y_i - y$ ). Inserting equation (12) into equation (16) and substituting the nominal value of  $r_o/t \approx 14.8$  gives

$$e = \frac{(y_i - y_o) (r_o^2/t^2 - 2r_o/t + 1)}{(2r_o/t - 1)} \approx 6.6(y_i - y_o) \quad (17)$$

Thus the resulting load eccentricity is over six times greater than the concentricity error. This illustrates the importance of maintaining concentricity (or equal material distribution around the strut circumference) during manufacture of the struts.

The minimum moment of inertia  $I$  for the eccentric cross section can be calculated by performing the appropriate area integral. The result is

$$I = \int_{Area} y^2 dA = \frac{\pi}{4} (r_o^4 - r_i^4) - \pi (y_i^2 r_i^2 - y_o^2 r_o^2) \quad (18)$$

The first term in this expression is the moment of inertia of the concentric cross section, and the second term is the reduction due to deviation from concentricity.

Substituting equations (12) through (16) into equation (18) and simplifying gives the equation for cross-sectional moment of inertia in terms of the outside radius, the average thickness, and the applied load eccentricity. This equation is

$$I = \frac{\pi}{4} [r_o^4 - (r_o - t)^4] - \pi e^2 r_o^2 \left[ \frac{r_o^2}{(r_o - t)^2} - 1 \right] = I_p - \pi e^2 r_o^2 \left[ \frac{r_o^2}{(r_o - t)^2} - 1 \right] \quad (19)$$

where  $I_p$  is the moment of inertia of the perfect cross section (one with no concentricity error). A concentricity error does not affect the area of the cross section, which is given by

$$A = \pi (r_o^2 - r_i^2) = \pi [r_o^2 - (r_o - t)^2] \quad (20)$$

Values for  $t$ ,  $\Delta t$ , and  $r_o$  were determined from averaged measurements made at each end of each specimen and values for  $e$ ,  $I$ ,  $I_p$ , and  $A$  were calculated for each specimen using equation (17), equation (11), and equation (12). A summary of these measured and calculated values as well as a list of the nominal design values for comparison are presented in table II.

Table II. Average Cross-Sectional Parameters for Test Specimens

Specimen	$r_0$ , in.	$t$ , in.	$\Delta t$ , in.	$e$ , in.	$I$ , in <sup>4</sup>	$I_p$ , in <sup>4</sup>	$A$ , in <sup>2</sup>
Nominal	1.066	0.072	0.000	0.000	0.248	0.248	0.466
1	1.070	.089	.021	.056	.300	.302	.575
2	1.072	.088	.014	.037	.299	.301	.568
3	1.070	.086	.016	.044	.291	.293	.555
4	1.069	.085	.015	.042	.288	.289	.548
5	1.066	.091	.015	.038	.303	.304	.584
6	1.064	.087	.026	.070	.287	.291	.558
7	1.062	.074	.017	.055	.249	.251	.477
8	1.069	.092	.027	.068	.306	.310	.591
<sup>a</sup> 9	1.065	.093	.027	.067	.306	.309	.595
10	1.065	.084	.015	.042	.281	.283	.540
11	1.062	.084	.012	.034	.280	.281	.541

<sup>a</sup>Because of problems in the manufacture of specimen 9, it was possible to make these measurements at only one end; therefore, the values given do not represent a strut average.

On the average, these specimens were approximately 20 percent thicker than the nominal design, with as much as a 30-percent variation in thickness around any given cross section. However, the presence of errors in concentricity caused only 1-2 percent reductions in the moment of inertia. In the following section, results are presented from axial compression tests and analysis which illustrate the effect of these dimensional irregularities on the load-shortening behavior of the struts.

**Results from axial compression analyses and tests.** A value for the effective Young's modulus,  $E$ , for each specimen was determined by considering the initial slope of the experimental load-shortening curve of the specimen. With this value and the values for the dimensional parameters given in tables I and II, the specimen's theoretical load-shortening curve can be generated by solution of equation (9) or equation (10) for a series of load values. Equation (10) gives the axial shortening between the ends of the strut, and therefore cannot be used for comparison with the experimental data. Consequently, theoretical load-shortening curves were generated by numerical integration of equation (9).

The experimental load-shortening curve for each specimen was determined using the compression test setup previously described. During each test, the specimen was subjected to a slowly increasing compressive load while a real-time plot of the load-shortening curve became nearly zero. Data from these tests are plotted in figures 10 through 20 for specimens 1 through 11, respectively.

The initial slopes of these curves,  $EA/l^*$ , were used to determine experimental values for  $E$ . These values are presented in table III for each specimen along with calculated values for the Euler buckling load ( $P_e = \pi^2 EI/l^2$ ); the perfect cross section Euler buckling load ( $P_{ep} = \pi^2 EI_p/l^2$ ); and the normalized maximum loads achieved in each test,  $q_{max}$ . A comparison of  $P_e$  and  $P_{ep}$  in table III illustrates the small reduction in  $I$  (and consequently  $P_{ep}$ ) resulting from lack of concentricity. Differences in the cross-sectional dimensions and effective Young's modulus of different specimens led to 10 percent variations in Euler buckling loads and effective axial stiffnesses.

Table III. Results From Axial Compression Tests

Specimen	$E$ , psi	$P_e$ , lb	$P_{ep}$ , lb	$q_{max}$	$q_l$
1	$27.3 \times 10^6$	2088	2102	0.90	0.96
2	27.6	2108	2122	.80	.93
3	28.9	2141	2156	.86	.95
4	28.8	2106	2113	.83	.94
5	25.7	1979	1986	.89	.94
6	29.2	2134	2164	.72	.95
7	32.9	2083	2100	.83	.93
8	27.8	2166	2194	.87	.94
9	26.7	2080	2100	.91	.96
10	27.7	1011	1018	.77	.90
11	27.7	1014	1018	.84	.94

Also included in table III are load values  $q_l$  at which the linear load-shortening analysis differs from the nonlinear analysis by 2 percent. These values were determined from analyses presented in appendix B. None of the specimens were tested to a load level above these limiting values ( $q_{max} < q_l$ ). Thus, geometric nonlinearities were unimportant, and the linear load-shortening analysis presented in equation (9) and equation (10) is applicable.

The theoretical load-shortening curves as determined from numerical integration of equation (9) are shown in figures 10 through 20. Good agreement is seen between the theoretical and experimental curves for all of the specimens except 4, 6 and 9. The specimens that had the greatest rms error in the parabolic approximation of their imperfections (specimens 1 and 3) showed reasonably good agreement between the theoretical and experimental load-shortening curves. Therefore, the poor agreement for specimens 4, 6, and 9 may be due to variations in their cross-sectional dimensions near the midspan. The cross-sectional dimensions in table II were determined from measurements made near the ends of the specimens (only one end for specimen 9); thus, any significant cross-sectional variations near the middle of the strut would not be represented in these measurements.

Initial imperfections and errors in cross-sectional concentricity significantly degraded the load-shortening behavior of all specimens as evidenced by the fact that all the specimens deviated markedly from linear elastic behavior characteristic of a corresponding perfect strut. This implies that control of cross-sectional concentricity and strut straightness is very important to achieve satisfactory performance from long slender truss struts.

### Concluding Remarks

The results of a study of the load-shortening behavior of initially imperfect struts under the action of eccentrically applied compressive loads have been presented. Linear analysis has been performed and compared with experimental results from 11 developmental aluminum-clad graphite/epoxy truss struts. These comparisons showed good agreement for most specimens.

The specimens were measured to determine deviations from straightness and nominal cross-sectional dimensions. These measurements were used to calculate values for initial imperfection magnitude and load eccentricity, as well as cross-sectional area and moment of inertia. It was determined that the load eccentricity resulting from an error in cross-sectional concentricity is over six times greater than the concentricity error.

Deviations from concentricity coupled with initial imperfections in straightness led to significantly degraded load-shortening behavior for all specimens tested. This illustrates the importance of maintaining concentricity and straightness during the manufacture of the struts.

## Appendix A

### Axial Shortening of an Eccentrically Loaded Strut With a Half-Sine Initial Imperfection

The half-sine initial imperfection given in equation (A1) is commonly selected for linear imperfect strut analysis because it is the same shape as the homogeneous solution to the governing differential equation (see eq. (1)). The solution for axial shortening of an eccentrically loaded strut with this initial imperfection follows the same steps as outlined for the parabolic initial imperfection.

$$w_o = \varepsilon \sin \frac{\pi x}{l} \quad (\text{A1})$$

Substituting equation (A1) into equation (1), determining the particular solution, and applying the boundary conditions results in the following expression for lateral displacement of an eccentrically loaded strut with a half-sine initial imperfection:

$$w(x) = \frac{q\varepsilon}{1-q} \sin\left(\frac{\pi x}{l}\right) + \frac{e}{\cos(\pi\sqrt{q}/2)} \cos\left(\frac{\pi\sqrt{q}}{2} - \pi\sqrt{q}\frac{x}{l}\right) - e \quad (\text{A2})$$

Equation (8) is evaluated by substitution of the half-sine initial imperfection  $w_o$  given in equation (A1) and the corresponding lateral displacement  $w$  given in equation (A2). The following integral expression is obtained for the axial shortening between any two points  $x_0$  and  $x_1$  of the strut:

$$\begin{aligned} \delta = \frac{1}{2} \int_{x_0}^{x_1} & \left\{ \left( \frac{\varepsilon\pi}{l} \right)^2 \left[ \frac{1}{(1-q)^2} - 1 \right] \cos^2\left(\frac{\pi x}{l}\right) + \left[ \frac{2e\varepsilon\pi^2\sqrt{q}}{(1-q)^2 \cos(\pi\sqrt{q}/2)} \right] \sin\left(\frac{\pi\sqrt{q}}{2} - \frac{\pi\sqrt{q}x}{l}\right) \cos\left(\frac{\pi x}{l}\right) \right. \\ & \left. + \left[ \frac{e\pi\sqrt{q}}{l\cos(\pi\sqrt{q}/2)} \right]^2 \sin^2\left(\frac{\pi\sqrt{q}}{2} - \frac{\pi\sqrt{q}x}{l}\right) \right\} dx + \frac{Pl^*}{EA} \end{aligned} \quad (\text{A3})$$

The total axial shortening of the strut can be determined by setting  $x_0 = 0$  and  $x_1 = l$  (thus  $l^* = l$ ) in equation (A3). The result is

$$\delta = \varepsilon^2 \left[ \frac{\pi^2}{4l(1-q)^2} - \frac{\pi^2}{4l} \right] + \varepsilon e \left[ \frac{2\pi q}{l(1-q)^2} \right] + e^2 \left\{ \frac{\pi\sqrt{q} [\pi\sqrt{q} - \sin(\pi\sqrt{q})]}{2l [1 + \cos(\pi\sqrt{q})]} \right\} + \frac{Pl}{EA} \quad (\text{A4})$$

Recall that  $e$  is the load eccentricity,  $\varepsilon$  is the midlength magnitude of the half-sine imperfection, and  $q$  is the applied compressive load normalized to the Euler buckling load. Equation (A4) is the sum of four terms similar to those in equation (10). In fact, the third and fourth terms are identical to those in equation (10) because they account for the effects of load eccentricity and uniform axial compression, which are unchanged from the first case. The different assumptions for initial imperfection shape account for the differences in the first two terms of equation (10) and equation (A4).

## Appendix B

### Importance of Geometric Nonlinearities

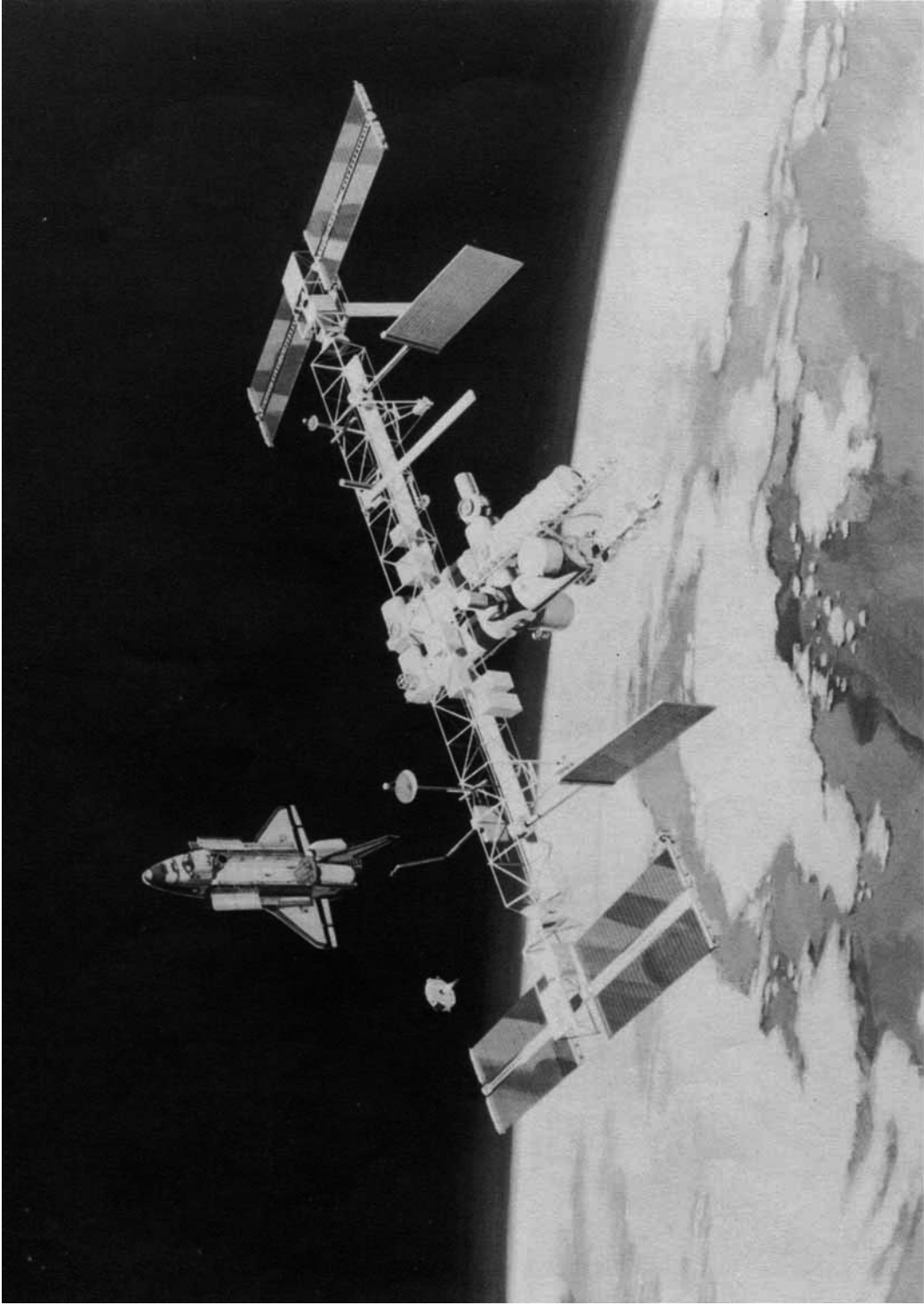
A recent study (ref. 9) has used the nonlinear formulation for axial compression of a strut (ref. 8) to investigate the load-shortening behavior of an eccentrically loaded strut with a constant-curvature (i.e., circular) initial imperfection. For small initial imperfection magnitudes, the parabolic shape presented in equation (4) closely approximates the circular shape assumed in the nonlinear analysis of reference 9. Thus, comparison of the linear solution presented in equation (10) with the corresponding nonlinear solution from reference 9 will identify the importance of geometric nonlinearities.

Linear analysis predicts larger deformations for large loads than those predicted with nonlinear analysis. From equation (10), it is evident that as  $q$  approaches 1, linear analysis predicts infinite axial shortening. However, nonlinear analysis predicts finite axial shortening for  $q = 1$ . The error in linear analysis increases with increasing load. Therefore, a load  $q_l$  at which the axial shortening from linear analysis is in error by a specified amount is defined as the limit of applicability of linear analysis.

Values for  $q_l$  can be determined for ranges of the strut parameters  $e/l$  and  $\varepsilon/l$  and general plots of this limiting load can be constructed. Figure 21 presents a carpet plot of  $q_l$  for an allowable error in linear analysis equal to 10 percent, and figure 22 presents a similar plot for an allowable error equal to 2 percent. These plots can be used to readily determine the limit of applicability of linear analysis for specimens with given values of  $e/l$  and  $\varepsilon/l$ . All experimental load-shortening data analyzed in the present study fall below the 2-percent-error limit for the respective specimen. Therefore, errors in linear analysis due to geometric nonlinearities are less than 2 percent.

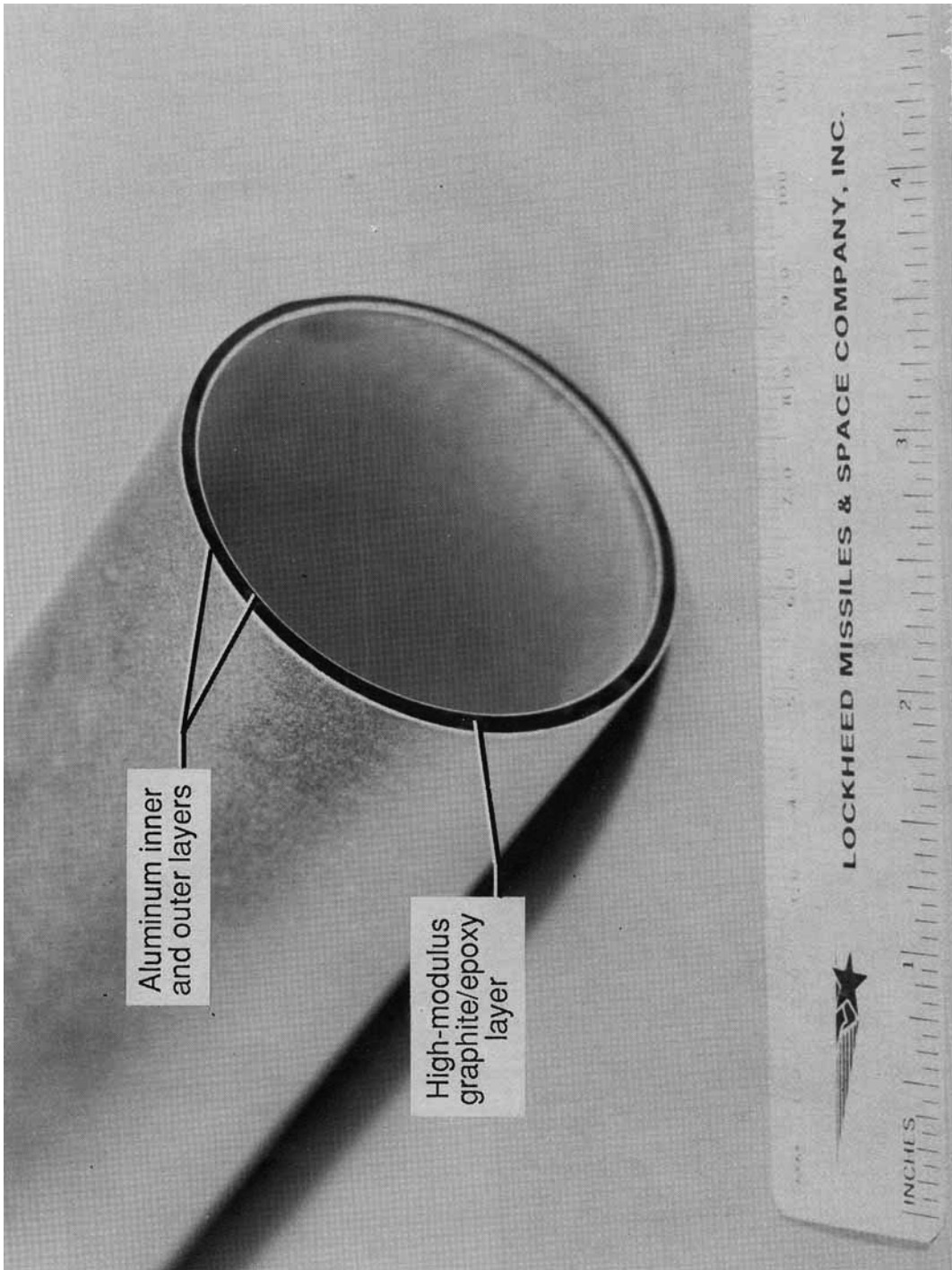
## References

1. Mikulas, Martin M., Jr.; Croomes, Scott D.; Schneider, William; Bush, Harold G.; Nagy, Kornell; Pelischek, Timothy; Lake, Mark S.; and Wesselski, Clarence: *Space Station Truss Structures and Construction Considerations*. NASA TM-86338, 1985.
2. Mikulas, Martin M., Jr.; and Bush, Harold G.: *Design, Construction and Utilization of a Space Station Assembled From 5-Meter Erectable Struts*. NASA TM-89043, 1986.
3. Johnson, R. R.; Bluck, R. M.; Holmes, A. M. C.; and Kural, M. H.: Development of Space Station Strut Design. *Materials Sciences for the Future - 31<sup>st</sup> International SAMPE Symposium and Exhibition*, Jerome L. Bauer and Robert Dunaetz, eds., Soc. for the Advancement of Material and Process Engineering, 1986, pp. 90-102.
4. Ring, L. R.: *Process Development and Fabrication of Space Station Type Aluminum-Clad Graphite Epoxy Struts*. NASA CR-181873, 1990.
5. Heard, Walter L., Jr.; Bush, Harold G.; Watson, Judith J.; Spring, Sherwood C.; and Ross, Jerry L.: Astronaut/EVA Construction of Space Station. *A Collection of Technical Papers — AIAA SDM Issues of the International Space Station*, Apr. 1988, pp. 39-46 (Available as AIAA-88-2459.)
6. Heard, W. L., Jr.; Bush, H. G.; and Agranoff, Nancy: *Buckling Tests of Structural Elements Applicable to Large Erectable Space Trusses*. NASA TM-78628, 1978.
7. Razzaq, Zia; Voland, R. T.; Bush, H. G.; and Mikulas, M. M., Jr.: *Stability, Vibration, and Passive Damping of Partially Restrained Imperfect Columns*. NASA TM-85697, 1983.
8. Timoshenko, Stephen P.; and Gere, James M.: *Theory of Elastic Stability*, Second ed. McGraw-Hill Book Co., 1961.
9. Fichter, W. B.; and Pinson, Mark W.: *Load-Shortening Behavior of an Initially Curved Eccentrically Loaded Column*. NASA TM-101643, 1989.



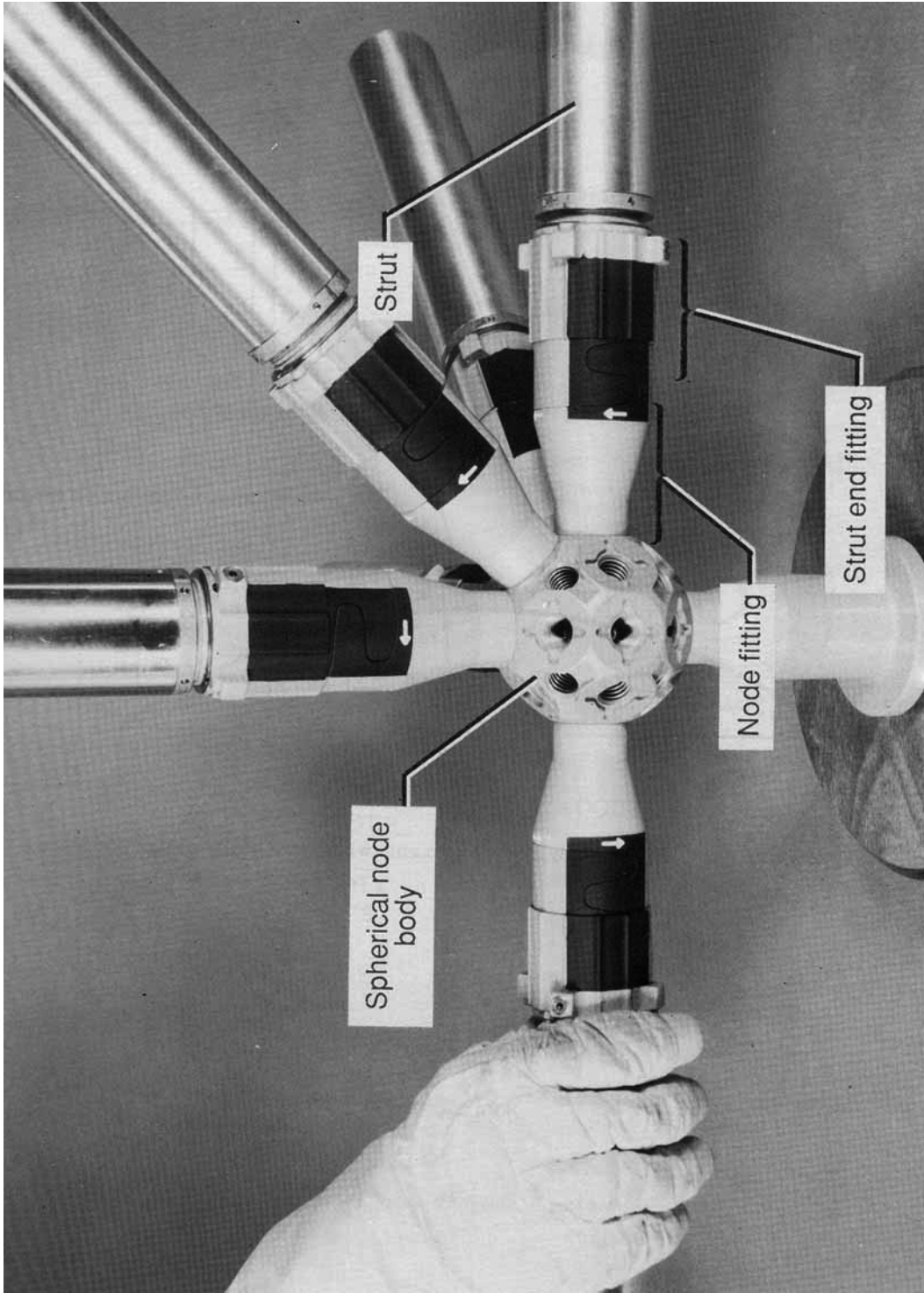
L-89-155

Figure 1. Space Station Freedom.



L-89-156

Figure 2. Aluminum-clad graphite/epoxy strut.



L-89-157

Figure 3. Quick-attachment erectable joint.

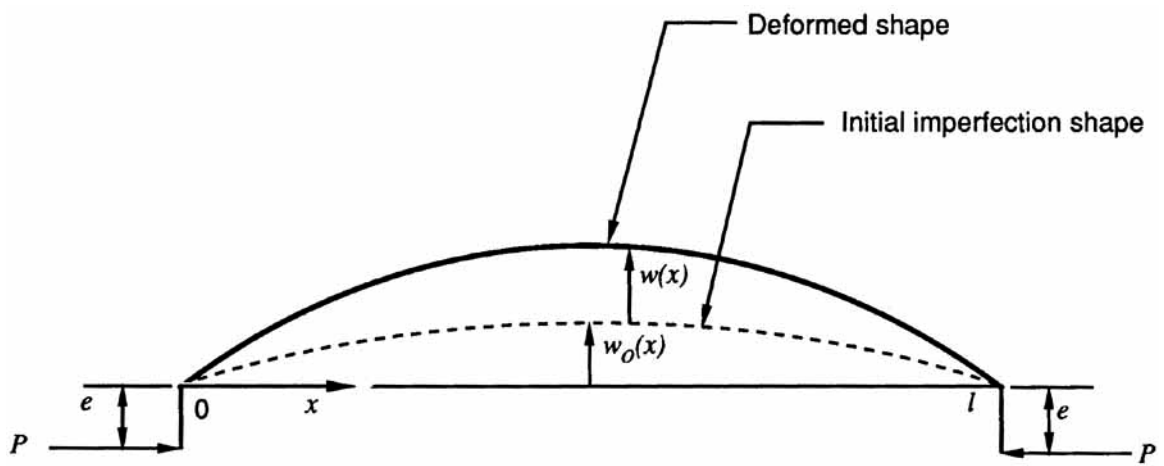


Figure 4. Axial compression of an initially imperfect column with eccentrically applied loads.

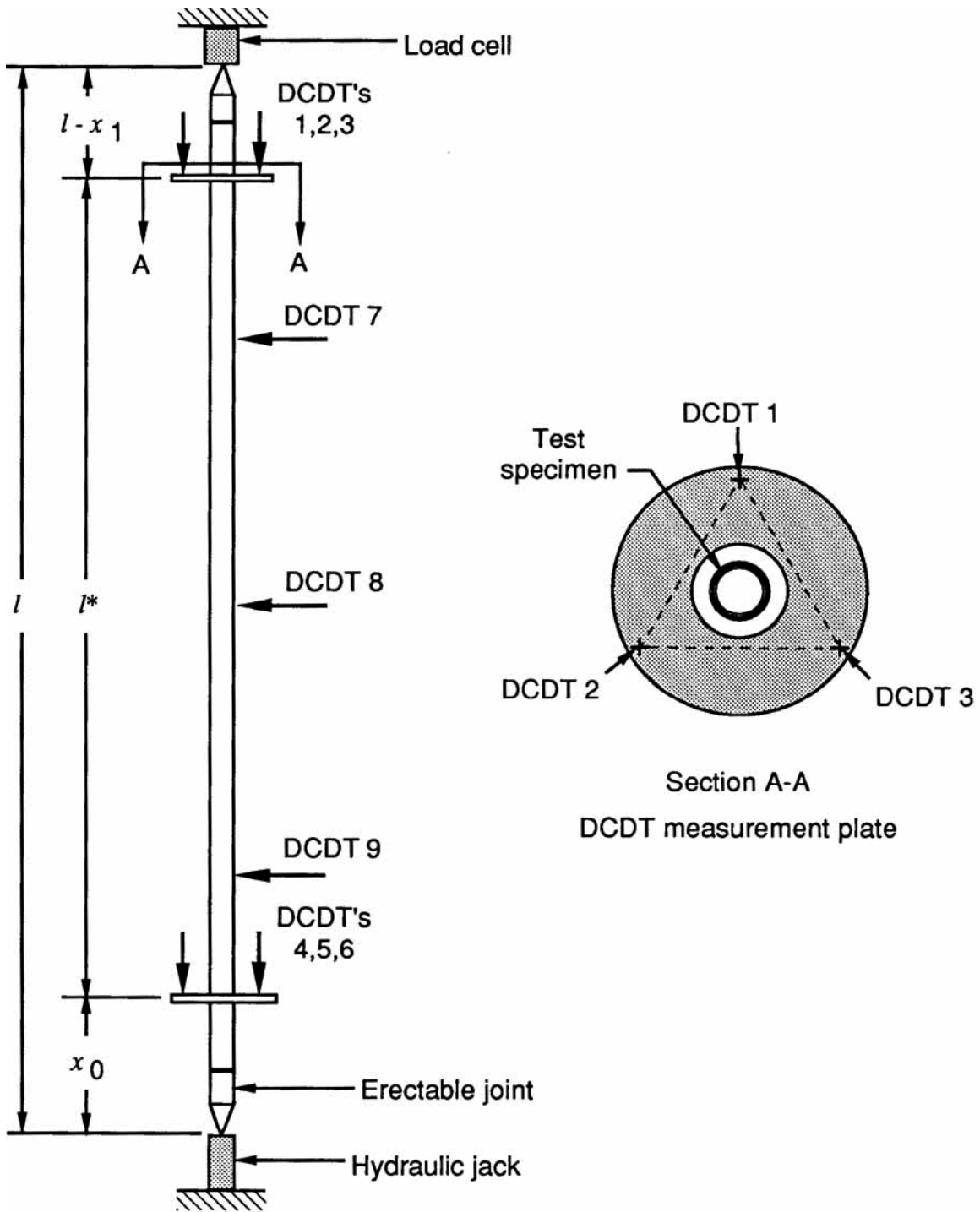
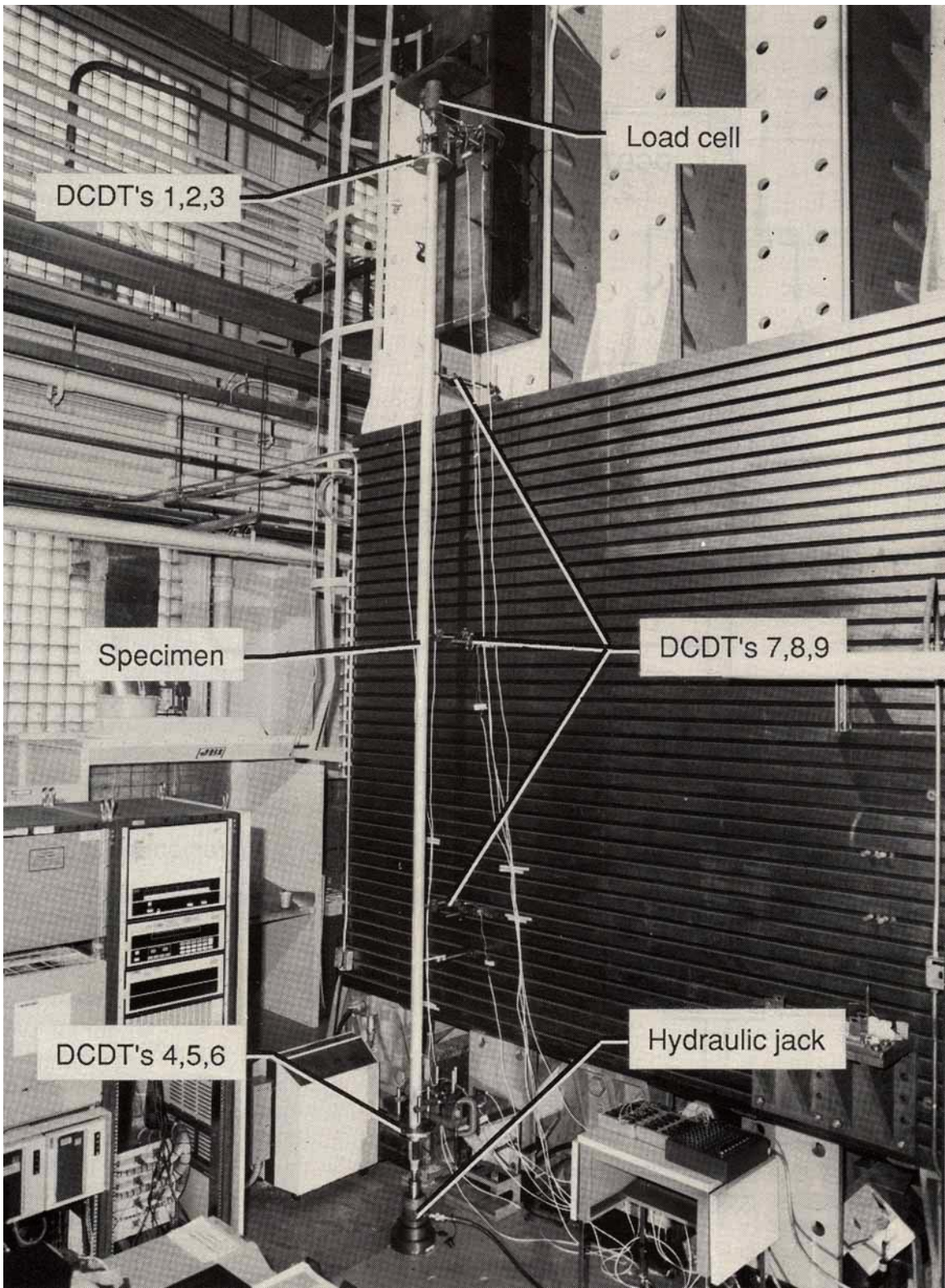


Figure 5. Diagram of test setup.



L-89-163

Figure 6. Test setup.

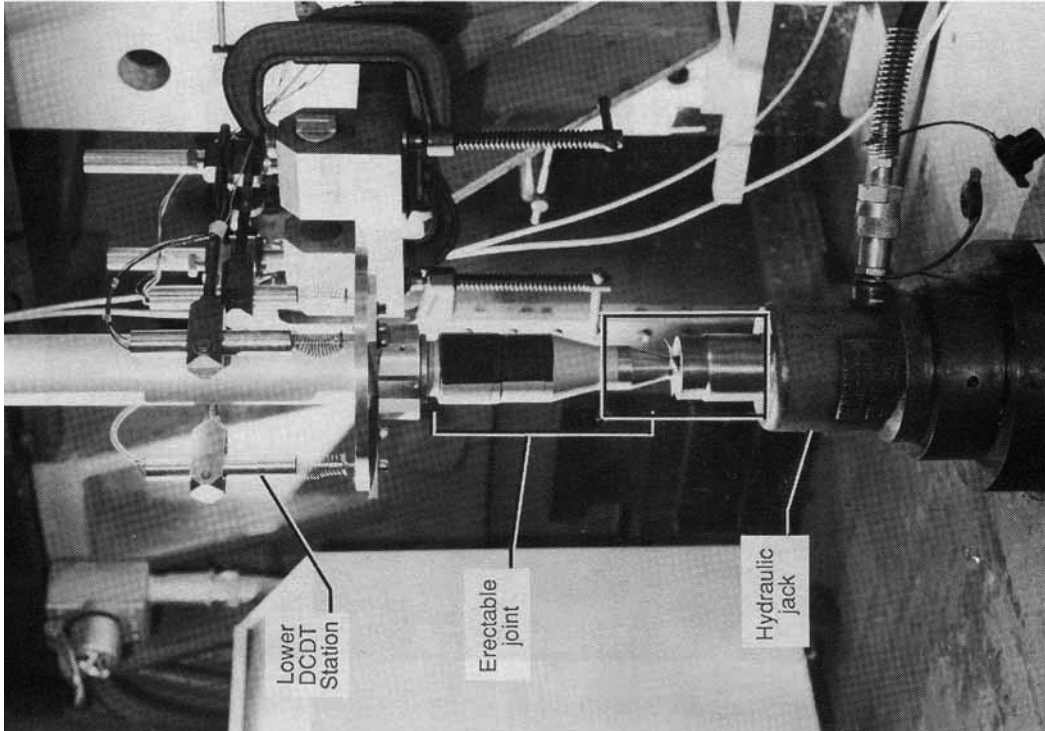
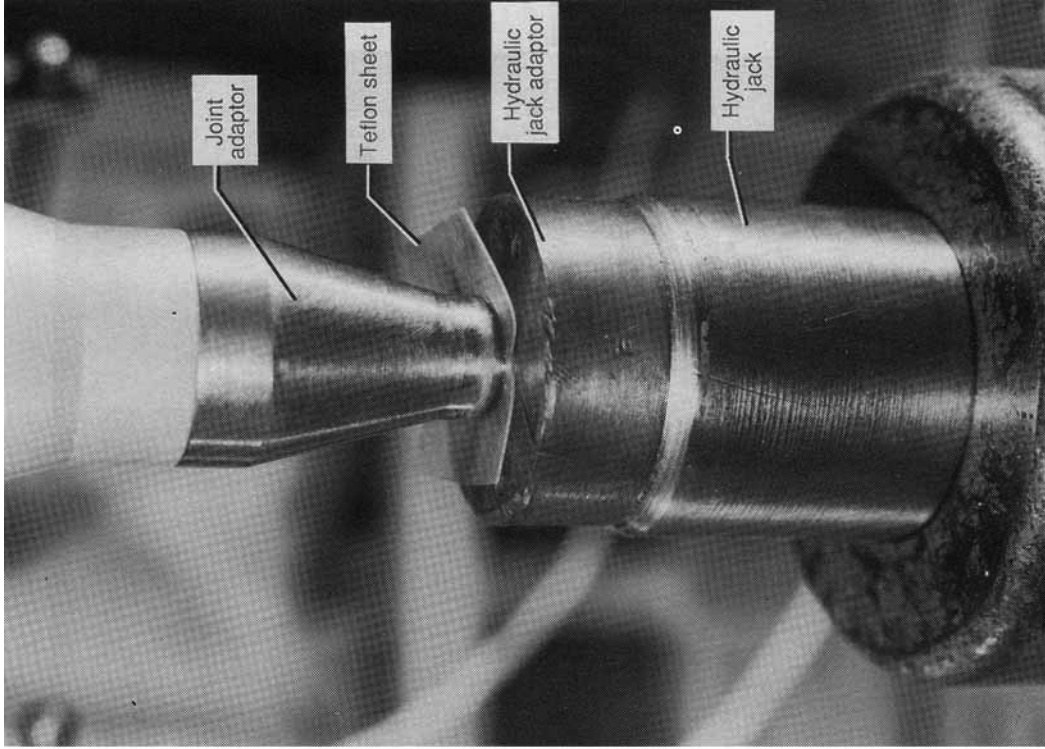


Figure 7. Specimen fixture detail.

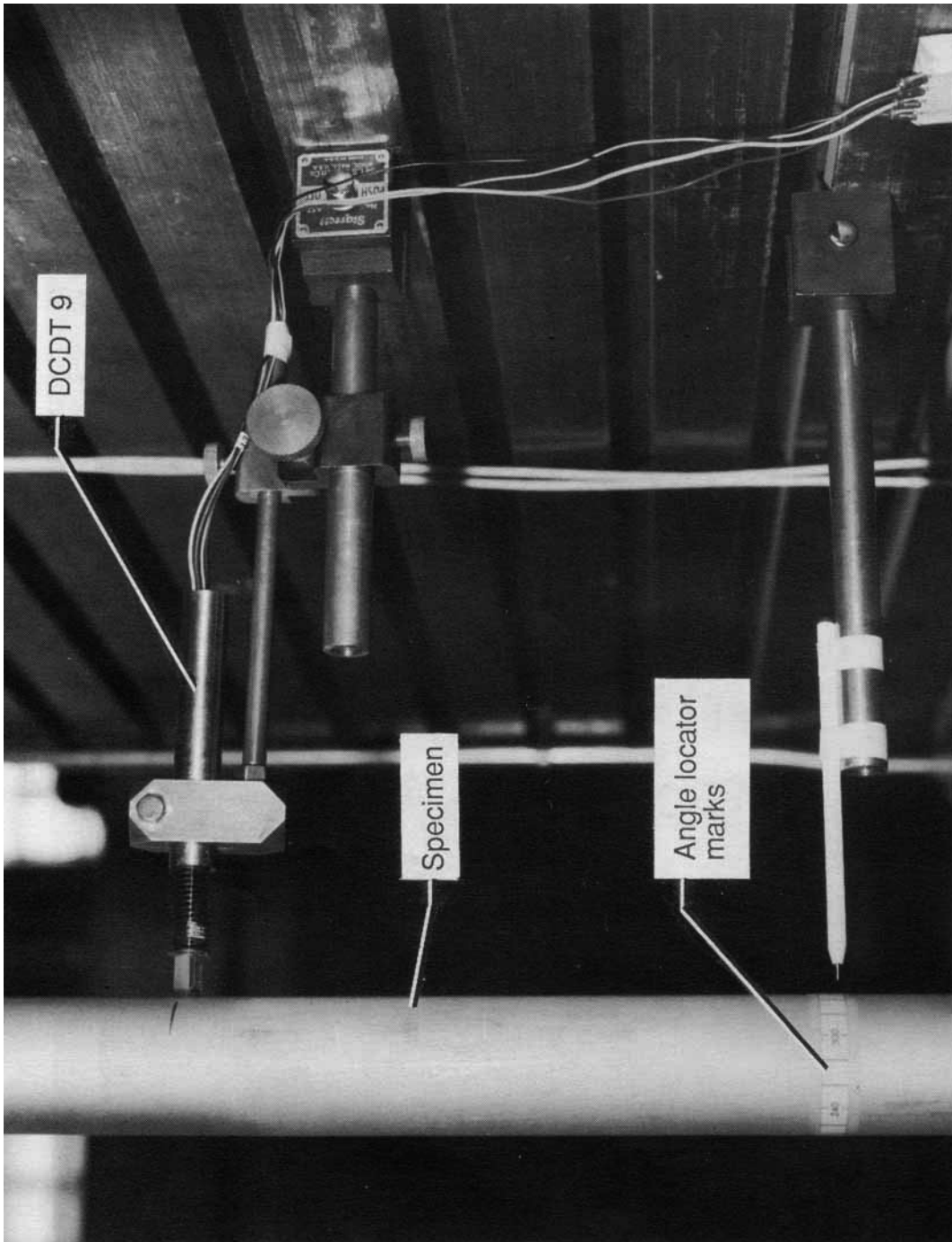


Figure 8. Initial imperfection measurement setup.

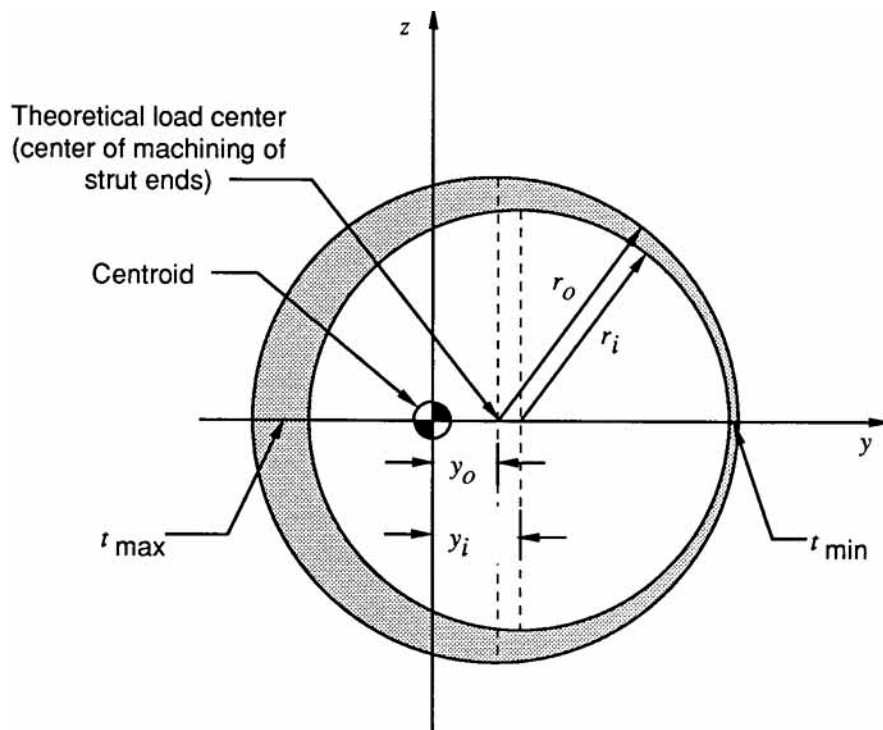


Figure 9. Nonconcentric strut cross section.

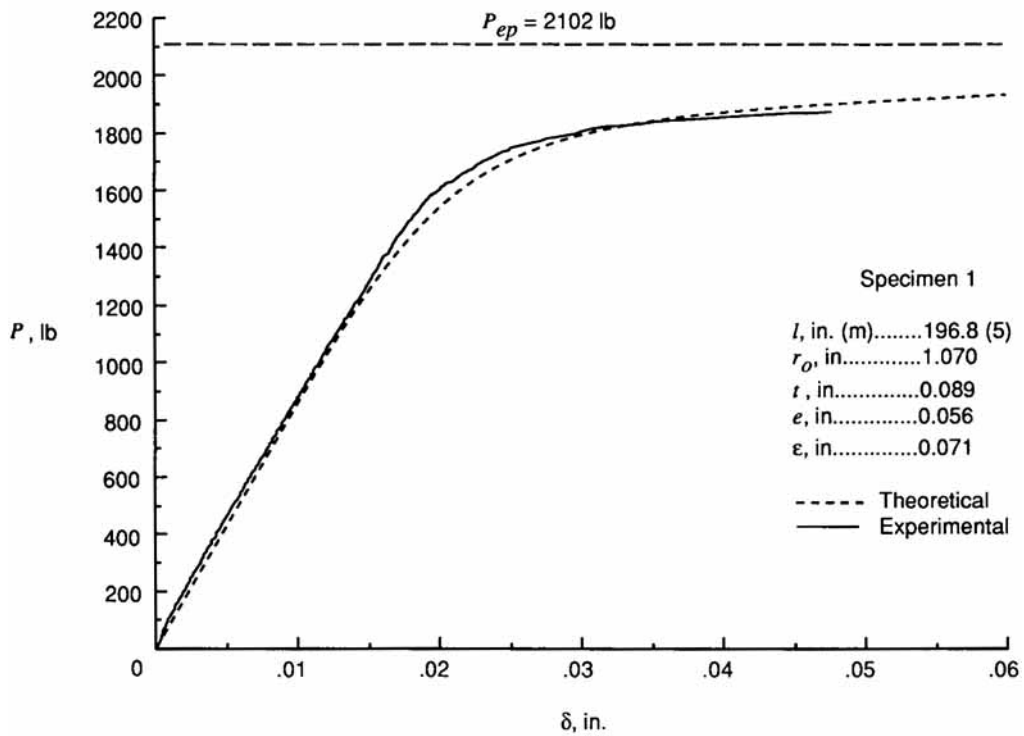


Figure 10. Load-shortening curve for specimen 1.

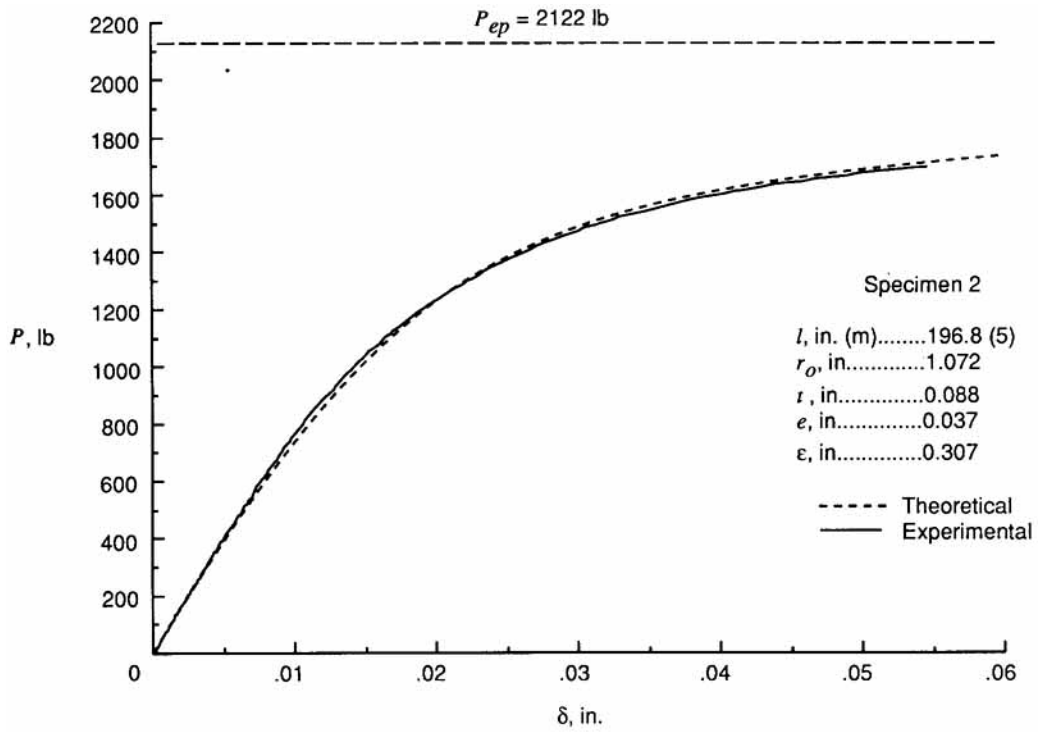


Figure 11. Load-shortening curve for specimen 2.

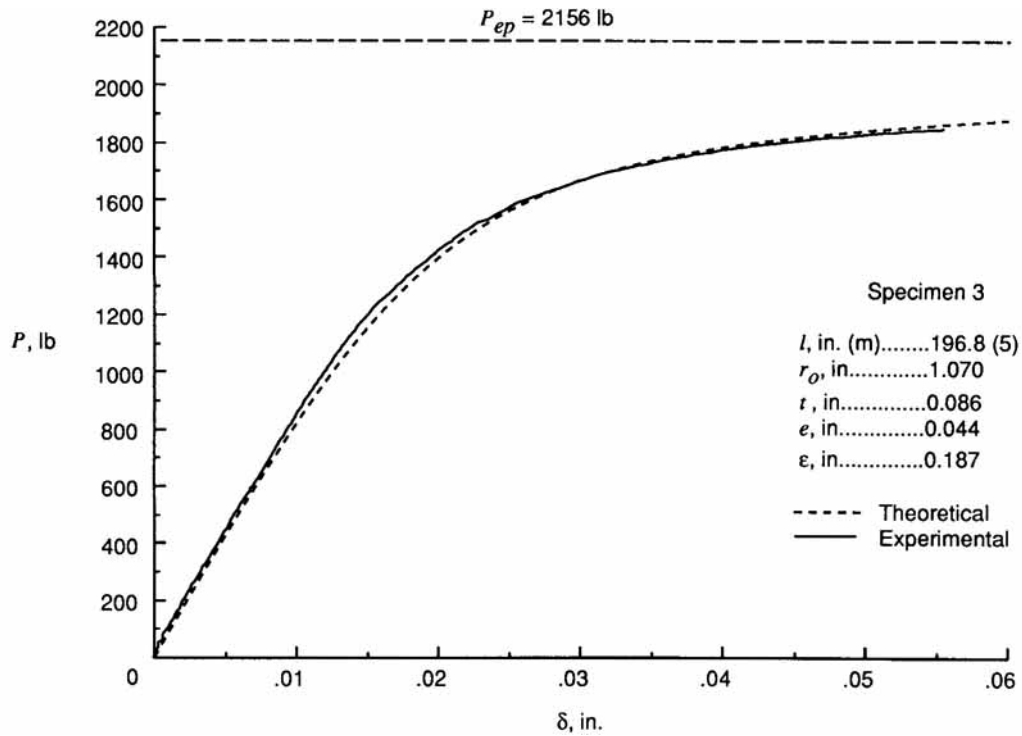


Figure 12. Load-shortening curve for specimen 3.

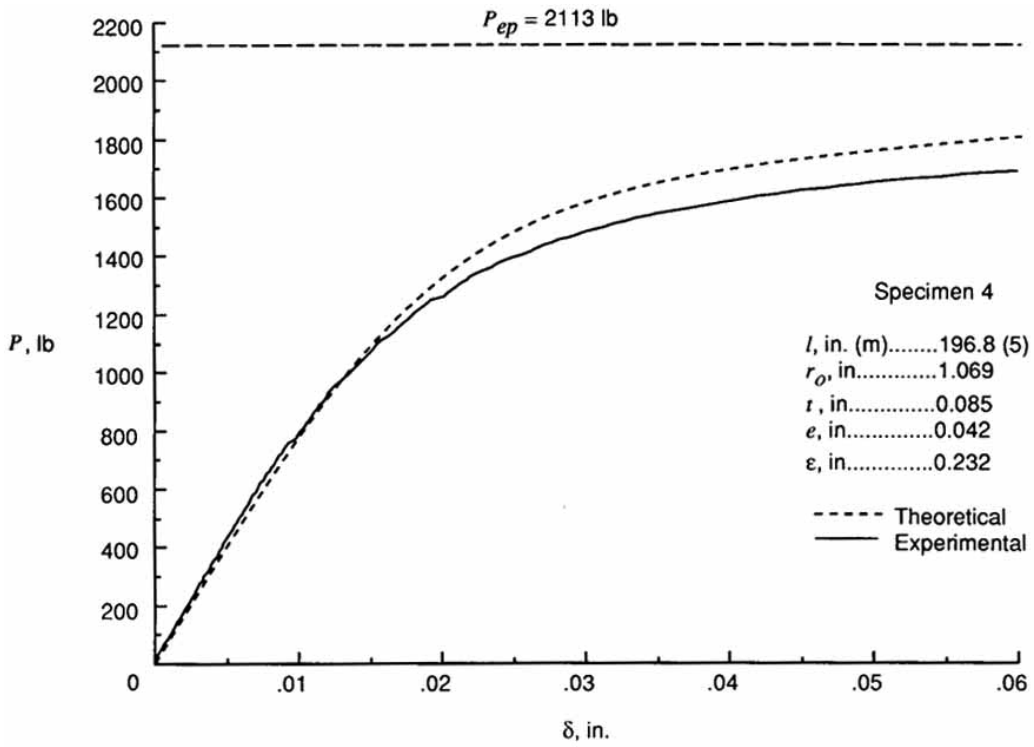


Figure 13. Load-shortening curve for specimen 4.

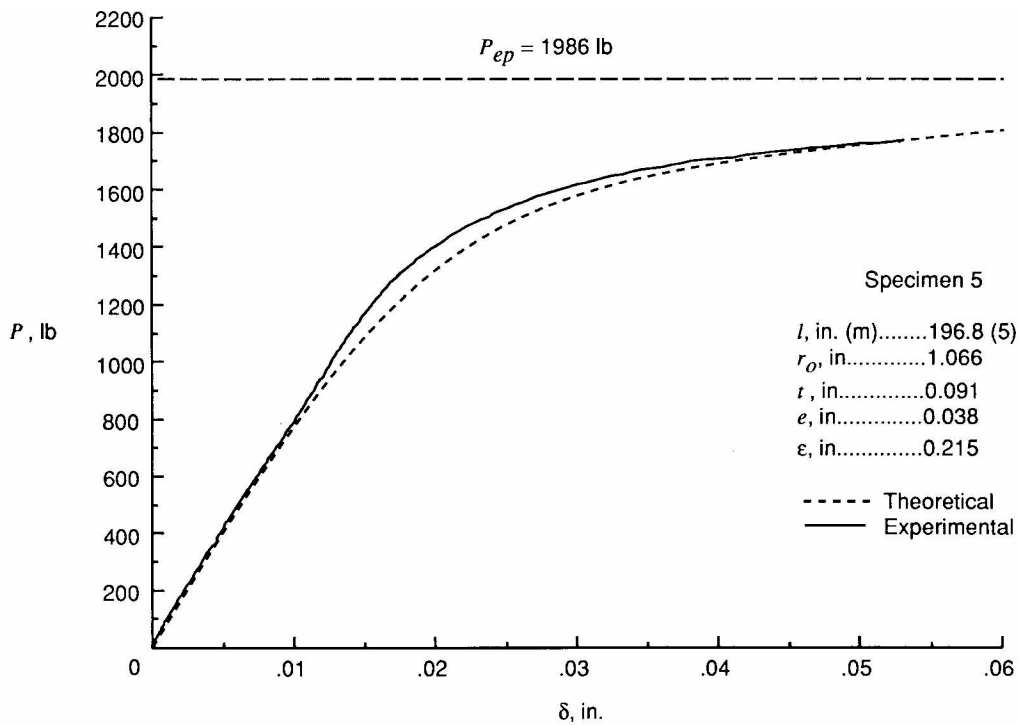


Figure 14. Load-shortening curve for specimen 5.

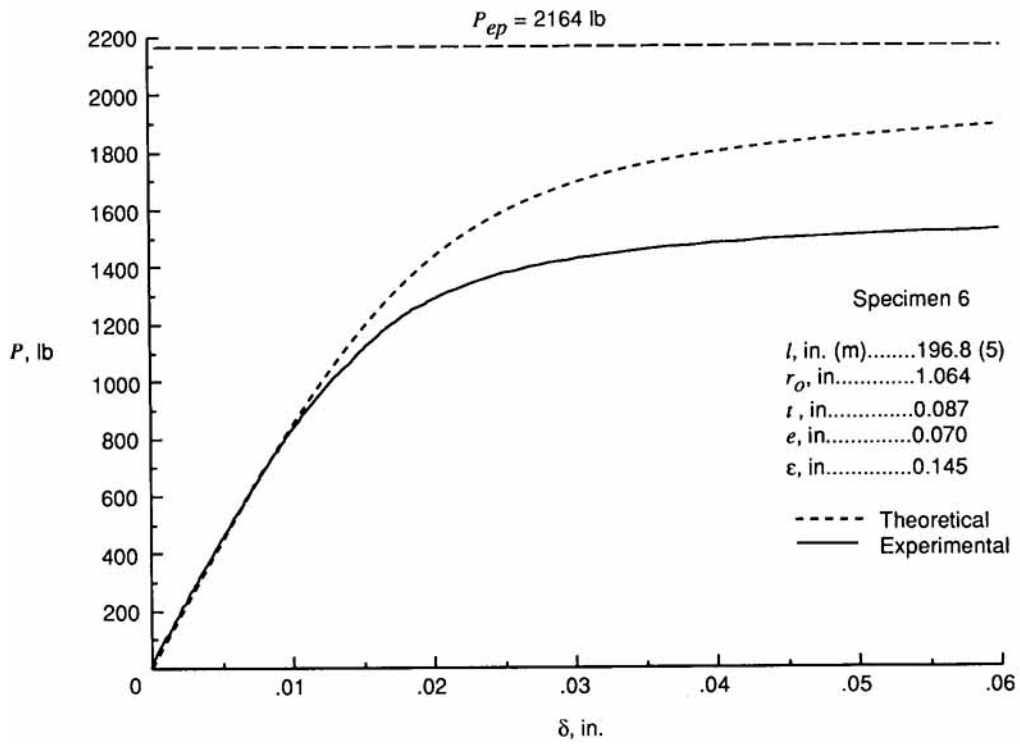


Figure 15. Load-shortening curve for specimen 6.

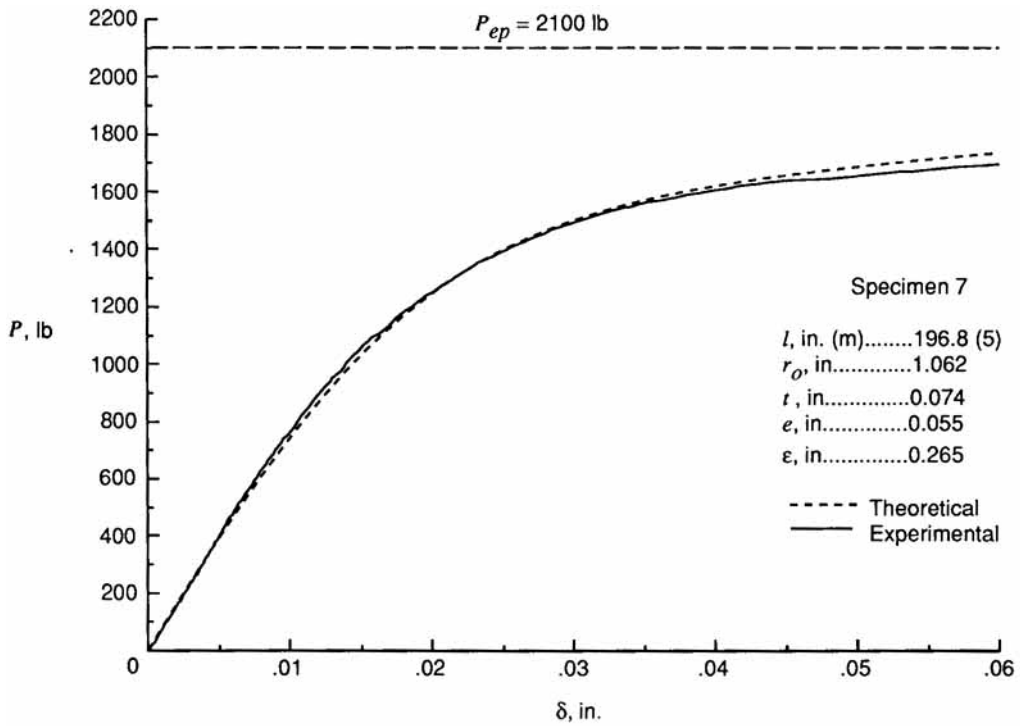


Figure 16. Load-shortening curve for specimen 7.

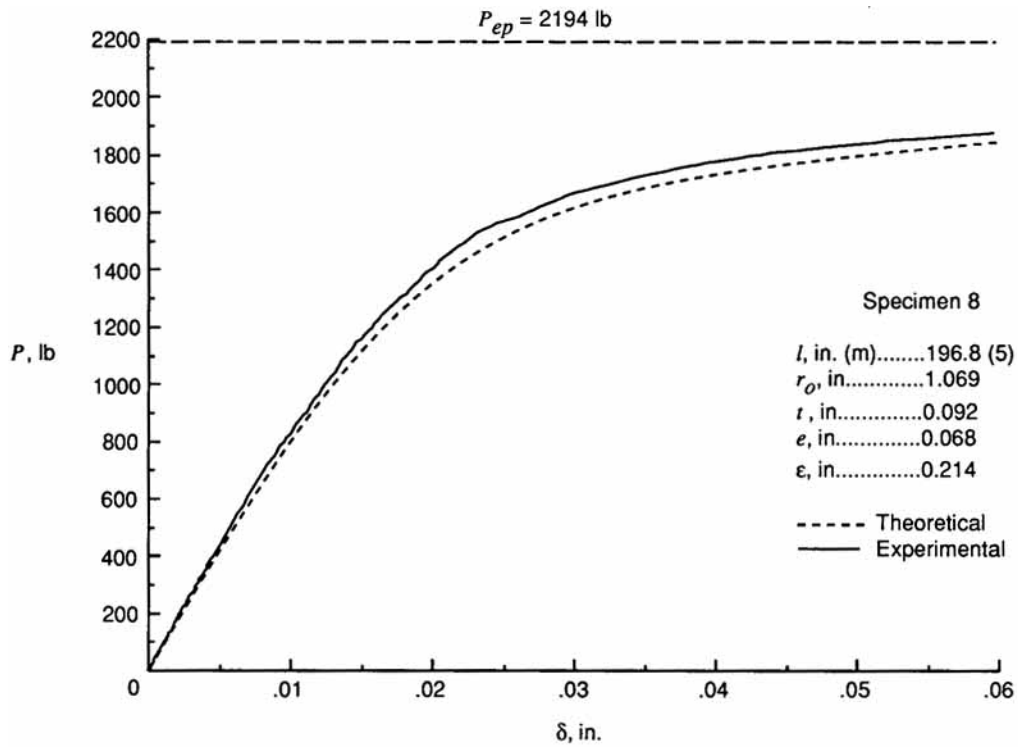


Figure 17. Load-shortening curve for specimen 8.

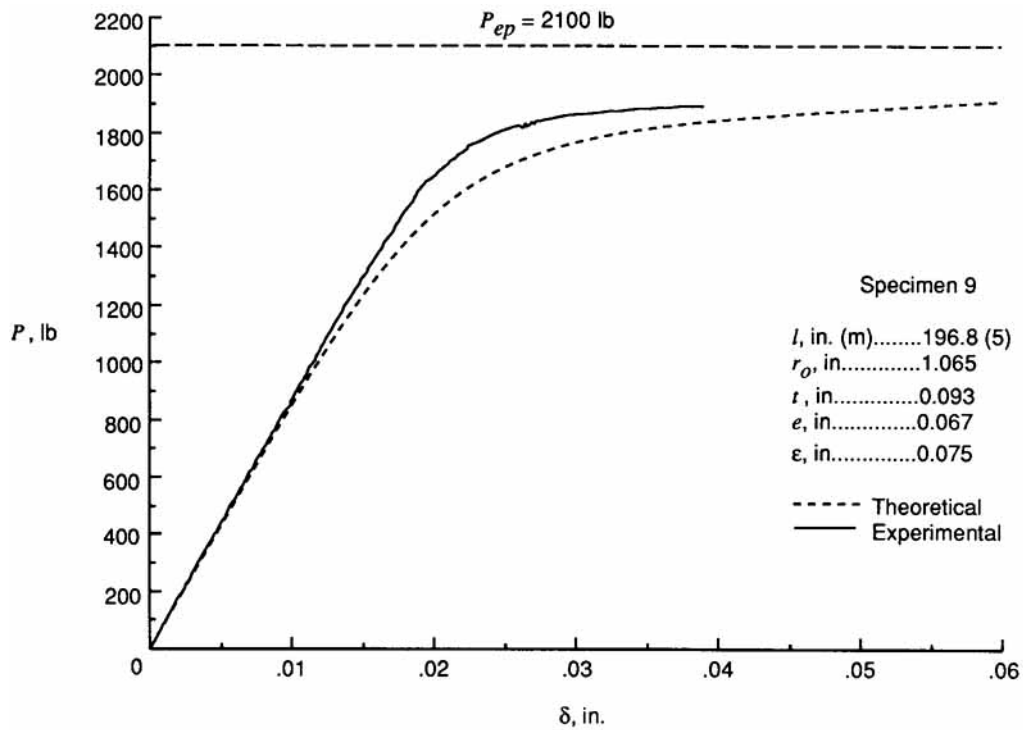


Figure 18. Load-shortening curve for specimen 9.

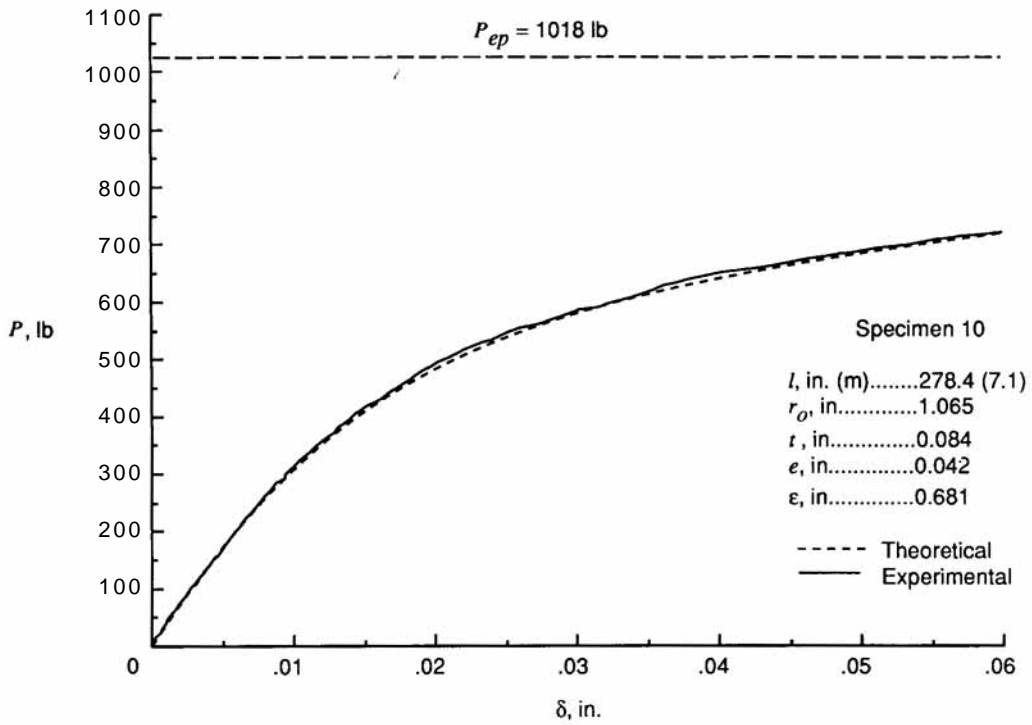


Figure 19. Load-shortening curve for specimen 10.

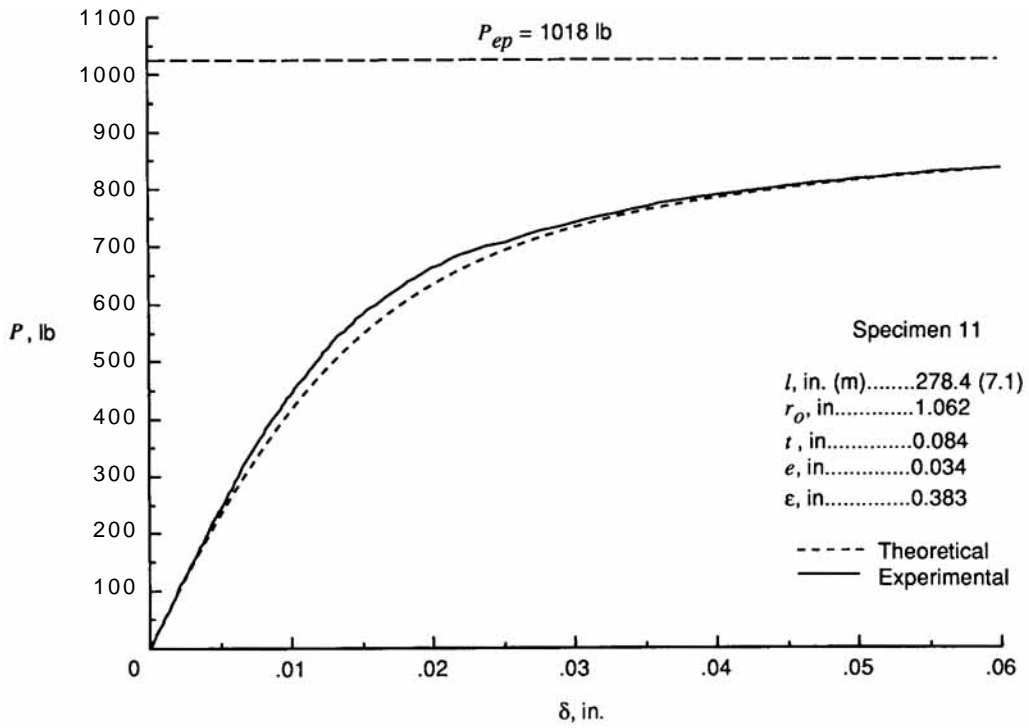


Figure 20. Load-shortening curve for specimen 11.

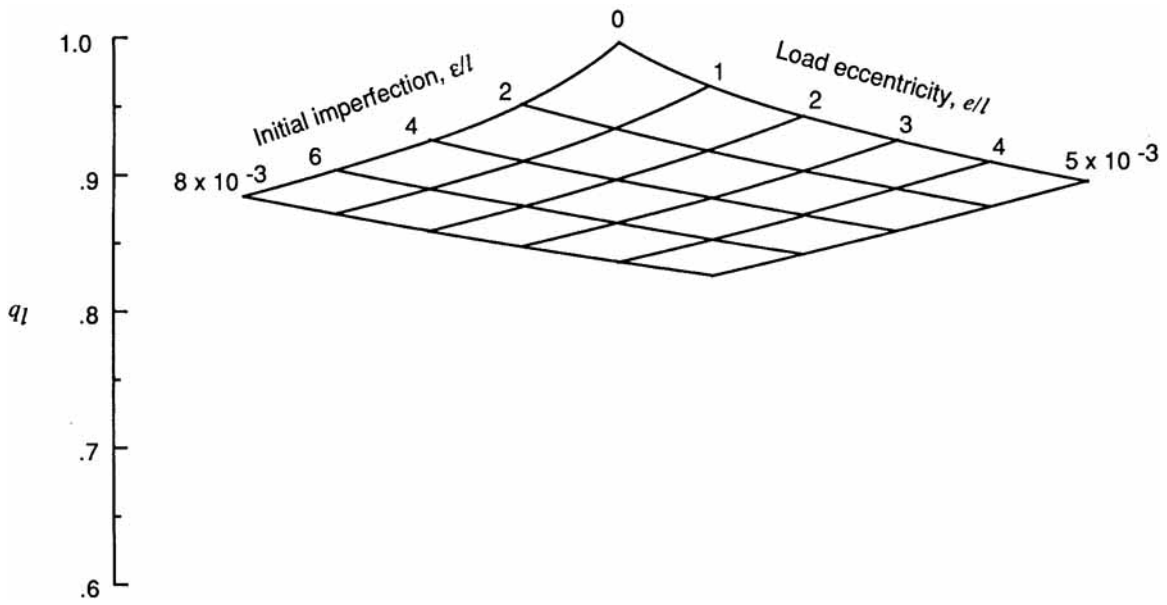


Figure 21. Limit of applicability of linear analysis (10 percent error in solution).

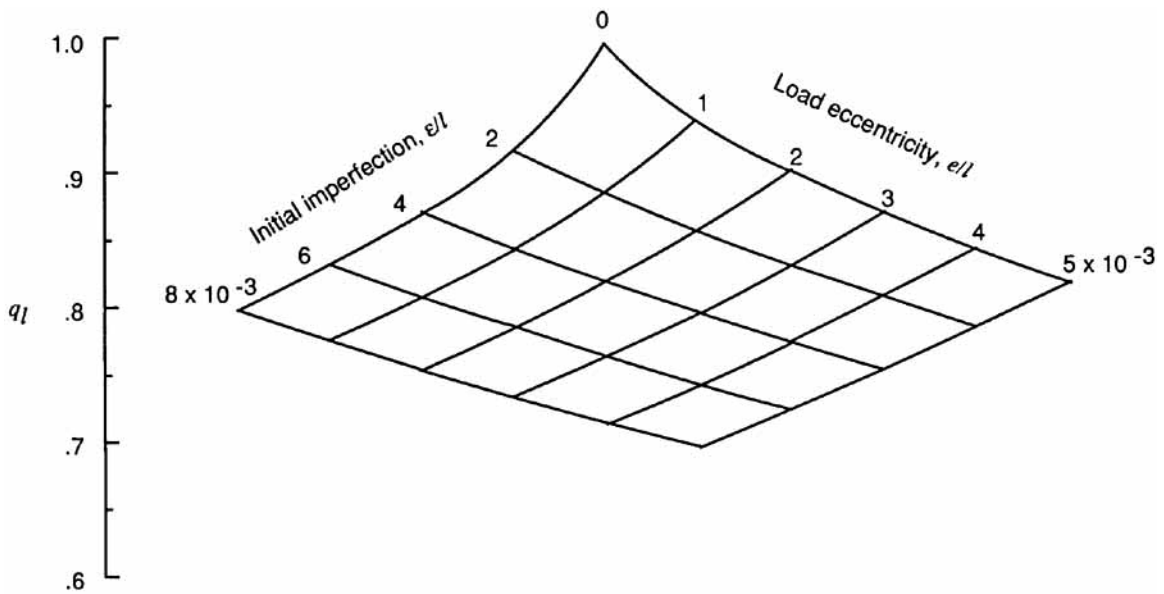


Figure 22. Limit of applicability of linear analysis (2 percent error in solution).



## Report Documentation Page

1. Report No. <b>NASA TM-4174</b>	2. Government Accession No.	3. Recipient's Catalog No.	
4. Title and Subtitle <b>Analysis and Testing of Axial Compression in Imperfect Slender Truss Struts</b>		5. Report Date <b>February 1990</b>	6. Performing Organization Code
		8. Performing Organization Report No. <b>L-16712</b>	
7. Author(s) <b>Mark S. Lake and Nicholas Georgiadis</b>		10. Work Unit No. <b>506-43-41-02</b>	11. Contract or Grant No.
9. Performing Organization Name and Address <b>NASA Langley Research Center Hampton, VA 23665-5225</b>		13. Type of Report and Period Covered <b>Technical Memorandum</b>	
		14. Sponsoring Agency Code	
12. Sponsoring Agency Name and Address <b>National Aeronautics and Space Administration Washington, DC 20546-0001</b>			
15. Supplementary Notes			
16. Abstract <p>This study addresses the axial compression of imperfect slender struts for large space structures. The load-shortening behavior of struts with initially imperfect shapes and eccentric compressive end loading is analyzed using linear beam-column theory and results are compared with geometrically nonlinear solutions to determine the applicability of linear analysis. A set of developmental aluminum-clad graphite/epoxy struts sized for application to the Space Station Freedom truss are measured to determine their initial imperfection magnitude, load eccentricity, and cross-sectional area and moment of inertia. Load-shortening curves are determined from axial compression tests of these specimens and are correlated with theoretical curves generated using linear analysis.</p>			
17. Key Words (Suggested by Author(s)) <b>Column stability Eccentricity load Initial imperfection Space station</b>		18. Distribution Statement <b>Unclassified-Unlimited</b>	
19. Security Classif. (of this report) <b>Unclassified</b>	20. Security Classif. (of this page) <b>Unclassified</b>	21. No. of Pages <b>28</b>	22. Price <b>A03</b>